Processing of Ultrasonic Array Signals for Characterizing Defects. Part I: Signal Synthesis

Guillermo Rus, *Member, IEEE*, Shi-Chang Wooh, *Member, IEEE*, and Rafael Gallego, *Member, IEEE*

***Abstract*—This work presents a novel procedure to characterize damage using an array of ultrasonic measurements in a generalized model-based inversion scheme, which integrates the complete information recorded from the measurements. In the past, we proposed some idealized nondestructive evaluation test methods with emphasis on the numerical results, but it is necessary to develop the techniques in greater detail in order to apply the techniques to real conditions.**

Our detection principle is based on the measurement and inversion of frequency-domain data combined with a reduced set of output parameters. The approach is developed and tested for the case of an aluminum specimen with a synthetic array of point contact ultrasonic transmitters and receivers.

The first part of this two-part paper is focused on numerical synthesis of the experimental measurements using the boundary element method for a general ultrasonic propagation model. This part also deals with the deconvolution by comparing the data measured from the damaged and undamaged specimens. The deconvolution technique allows us to calibrate the data by taking into account the uncertainties due to mechanical properties, input signal, and other coherent noise. The second part of the paper presents the inversion of the measurements to obtain the parameters and ultimately to predict the position and size of the real defect.

I. Introduction

When we seek defects in a body, which is accessible only from some surfaces, we normally use a form of energy propagating into the body and analyze the signal returned from the body to the accessible surface. In this work, we utilize high frequency acoustic energy, i.e., ultrasound, and its response with respect to the structure inside the test material. We use the response data to derive the condition of damage and the strength of the material, which is an ultimate goal of a nondestructive evaluation (NDE) technique.

Model-based NDE is the most advanced technique to process the experimental measurements. Our goal is to synthesize a valid numerical signal that matches the experimental counterpart. The synthesized signal is then used in the second part to illustrate the inversion strategy based on the minimization of the discrepancies between the measured and the synthesized data.

Model-based studies of ultrasonic transducers can be found in a host of reference articles. The *Nondestructive Testing Handbook* [1] reviews the basic theories of transducer modeling. Marty *et al.* [2] show the experimental results for Lamb waves in plates and thickness variations, in which they model the transducers as point sources and the receivers set in pulse-echo mode. Wendel *et al.* [3] demonstrated the concept of numerical simulation combined with experiments for training the neural networks. Some pieces of software have been developed in recent years, all of which use semi-analytical components, such as CEA-Calmon [4], CNDE-Thompson, or UTDefect-Bostrom [5].

Some investigators, e.g., Kimoto and Hirose [6], point out the problems associated with the simple boundary conditions. They proposed a model in which the transmitting transducers are modeled as a distribution of tractions and the receivers are represented by a weighted displacement function. They use the boundary element method to compute the ultrasonic response of the specimen. Such tools are adopted to model the transmission testing of our setup. We also included in our study a transfer function of the transducer-specimen system. The transfer function, well described by Schmerr [7], is a time-shift invariant (LTI), which is basically a Green's function used to average the values within the transducer surface. Using these techniques, it is possible to reduce the discrepancy between the experimental and the numerical signals down to the order of 20% of the maximum signal. Averaging of computations enhances the results. This gives an idea of the state-of-the-art limitations in forward models for real nondestructive technology situations, and the intrinsic complexity of the problem.

Zhao *et al.* [8] used the velocity instead of the displacements to model the receiver. They compared their results with the other numerical methods studying the ultrasonic response of the specimen. They obtained the attenuation ratio experimentally for a thin sample.

It should be noted that the concept of one-point calibration may not be sufficient, especially for complex wave propagation patterns, as reported by Hill *et al.* [9] in their finite element model. Rus *et al.* [10] made an effort to correctly simulate the transducer considering the revised boundary conditions. The basis for this and the linearity of the system are revised in the present paper.

The main disadvantages to a large surface contact transducer include signal distortion, cutting-off of certain fre-

Manuscript received June 5, 2006; accepted May 25, 2007. We gratefully acknowledge the Fulbright Foundation and the *Ministerio de Educación, Cultura y Deporte* for the postdoctoral fellowship FU2002-0442 supporting this work.

R. Guillermo and S.-C. Wooh are with the NDE Laboratory, Department of Civil and Environmental Engineering, Massachusetts Institute of Technology, Cambridge, MA 02139 (e-mail: grus@ugr.es).

R. Gallego is with the Department of Structural Mechanics, University of Granada, Granada, Spain.

Digital Object Identifier 10.1109/TUFFC.2007.508

quency components, and the near field effects, which are referred to as the *aperture effects*. The benefits of using point sources and point receivers have been addressed by Sachse [11]. One of the ways to produce point contact between the contact transducer and the target surface is to use a miniature or pencil-tip transducer. Lee *et al.* [12] demonstrated a technique to achieve small contact surface areas in the order of 200 to 400 μm in diameter by directly cutting a piezoelectric plate using a laser beam. An easier way to provide point contact is to use a cylindrical cone or a triangular wedge, whose vertex or knife-edge is in contact with the surface while a normal-sized transducer is mounted on the flat surface of the wedge. The use of wedges to collimate waves and to generate point sources was first introduced by Ying in 1967 [13]. For this experiment, a triangular wedge of aluminum is introduced, whose analysis and design is addressed by Rus *et al.* [10].

The novel contributions in this paper can be summarized as the development of a procedure to synthesize a model-based signal for a transmission ultrasonic simulated array of point transmitters and receivers. This is in addition to the implementation of two calibration techniques, which allow us to overcome uncertainties in several exact model parameters, aimed at solving the inverse problem of defect characterization with a high computational efficiency.

II. NDE System Model

The first step in setting up the model is to define a system and its components. The generic system, shown in Fig. 1, consists of the four basic components: the signal generator, the transducers, the specimen, and the signal recorder. The transfer functions of these components are denoted by the respective capital superscripts I (Input), T (Transmitter), R (Receiver), and O (Output). The assumed hypotheses for the physical model are first established for the purpose of describing later the interactions between the components. Regarding the physical components, the following ones are differentiated in the model:

- **Specimen**. A block of material to be analyzed.
- **Transducers**. Transmitters, which are in charge of emitting an elastic wave into the specimen; and receivers, which record the received signals.
- **Oscilloscope**. Captures the received signals.
- **Waveform generator**. Generates electrical signals for the transmitters.

From the viewpoint of the traveling information, among the numerous ones, the following steps are of particular interest:

- $s_m^{(I)}(t)$: Input Signal. This is the signal emitted from the wave generator. In general, we use one input for each transmitter ($m = 1..N^m$).
- $s_m^{(T)}(t)$: Transmitted Signal. This is the signal emitted from the transmitter traveled through the specimen. We measure one signal for each transmitter (m).
- $s_{mn}^{(R)}(t)$: Received Signal. This is the signal that reaches the receiver. In general, for each receiver ($n = 1..N^n$) we make different signals for each transmitter (m).
- $s_{mn}^{(O)}(t)$: Output Signal. This is the signal recorded by the oscilloscope. As above, all combinations of transmitters (m) and receivers (n) are taken into account.

The relationships between these signals can be expressed in the time domain as follows:

$$\begin{aligned} s_{mn}^{(O)}(t) &= h_{mn}^{(RO)}(t) * s_{mn}^{(R)}(t), \\ s_{mn}^{(R)}(t) &= h_{mn}^{(TR)}(t) * s_{m}^{(T)}(t), \\ s_{m}^{(T)}(t) &= h_{m}^{(IT)}(t) * s_{m}^{(I)}(t), \end{aligned} \tag{1}$$

where the symbol $*$ means convolution of the two signals, and h represents transfer functions treated later.

A. Hypothesis for Transducers

- The transmitter is modeled as the prescribed pressure boundary conditions: $q_i(x,t)$. The validity of this assumption was studied by Rus *et al.* [10] by comparing the results between the two extreme cases of Neumann and Dirichlet boundary conditions.
- As commented on in the next section, the electrical and mechanical coupling at the transducer-specimen interface is taken into account in the linear transfer functions $h_m^{(IT)}(t)$ for the transmitter and $h_n^{(RO)}(t)$ for the receiver.
- We assume uniformly weighted pressure q_i over the surface resulting in in-phase and displacements u_i with the same amplitude distribution over the contact surface Γ_c: $q_i(x,t) = q_i f(t)$ for the transmitter and the average $u_i(t) = \int_{\Gamma_n} u_i(\Gamma,t)d\Gamma$ for the receiver.
- Only the normal components are considered: $s_m^{(T)}(t) = q_i(x,t)n_i$ for the transmitter and $s_{mn}^{(R)}(t) = u_i(t)n_i = \int_{\Gamma_n} u_i(\Gamma,t)d\Gamma n_i$ for the receiver.

B. The Electromechanical Response

In many practical applications, a dynamic system response can be measured using a commercial transducer such as a piezoelectric accelerometer or a displacement sensor which converts mechanical motions into electrical signals. The behavior of a transducer may be modelled by a complex electromechanical system by considering all of the design details of the system. However, a number of assumptions allow to simplify the model by establishing linear relationships. Linearity can be assumed as long as the magnitudes remain within a limited range of operation, which is our case.

We consider a transducer consisting of the linear components shown in Fig. 2, i.e., a piezoelectric plate, the damping material, and the casing. Such a transducer can be mechanically characterized by the following properties: The constant k_p is the stiffness of the piezoelectric plate, k_d, is the stiffness of the equivalent spring of the damper,

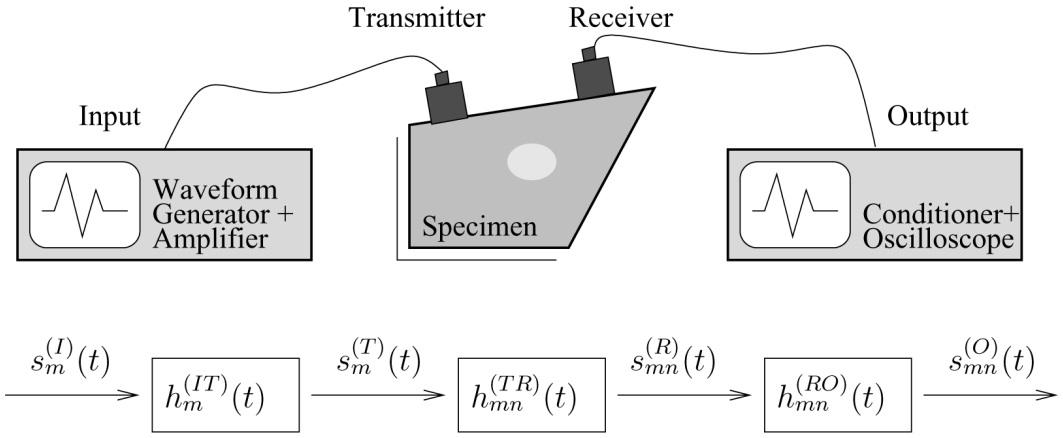

Fig. 1. Schematic decomposition of a typical NDE system. Grouping of signal classes and the transfer functions between them.

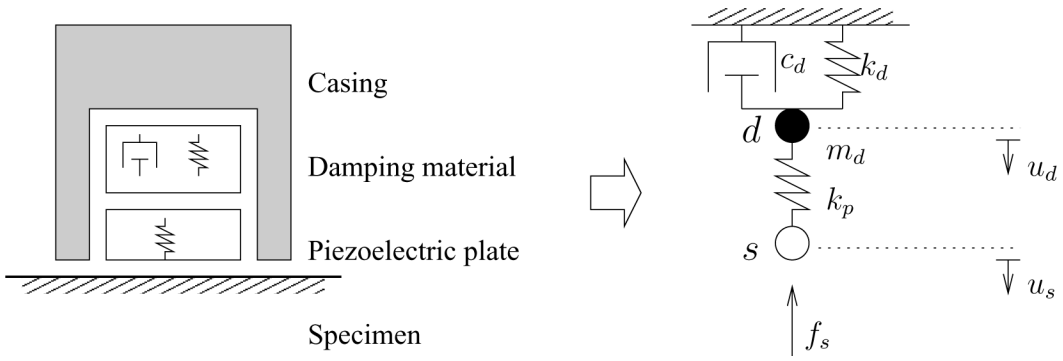

Fig. 2. Diagram of the physical transducer model considered for the current simplification.

c_d is the damping coefficient of the damper, m_d is the lumped mass attributed to the damper, and f_s is the force acting on the surfaces between the specimen and the transducer. The variables u_s and u_d denote the displacements of the specimen and the damper, respectively. Notice that these are the displacements of the two surfaces of the piezoelectric plate in the transducer. The pair $\{u_s, f_s\}$ defines the mixed boundary condition at the specimen-transducer contact area.

The equilibrium equation for this model can be written as

$$m_d\ddot{u}_d(t) + c_d\dot{u}_d(t) + k_d u_d(t) + k_p u_d(t) = k_p u_s(t). \tag{2}$$

It is noted that the displacement can be decomposed into the harmonics using the Fourier decomposition:

$$u(t) = \int_\omega U(\omega)e^{j\omega t}d\omega, \tag{3}$$

where ω is the angular frequency, $U(\omega)$ is the Fourier transform of $u(t)$, and j is the unit imaginary number. This model allows us to rewrite the equilibrium equations in the form

$$U_d(\omega) = A_1(\omega)U_s(\omega), \tag{4}$$

where

$$A_1(\omega) = \frac{k_p}{-m_d\omega^2 + jc_d\omega + k_d + k_p}, \tag{5}$$

and $A_i(\omega)$, the inverse transforms of $\alpha_i(t)$, are the complex constants in the sequel. The deformation of the piezoelectric plate can be expressed by the difference between the displacements of its surfaces as

$$U_d - U_s = A_2U_s, \tag{6}$$

where

$$A_2(\omega) = \frac{m_d\omega^2 - jc_d\omega - k_d}{-m_d\omega^2 + jc_d\omega + k_d + k_p}. \tag{7}$$

Without losing the generality, the output signal $s_{mn}^{(O)}(t)$ produced by the piezo-material can be assumed to be linearly proportional to the deformation through a constant A_3 as follows:

$$s_{mn}^{(O)}(t) = A_3(u_d - u_s). \tag{8}$$

From (6), this can be simply written as

$$s_{mn}^{(O)}(t) = A_4u_s, \quad A_4 = \mathcal{F}^{-1}\{A_2A_3\}. \tag{9}$$

This means that the relationship between the displacements can be numerically modeled without considering

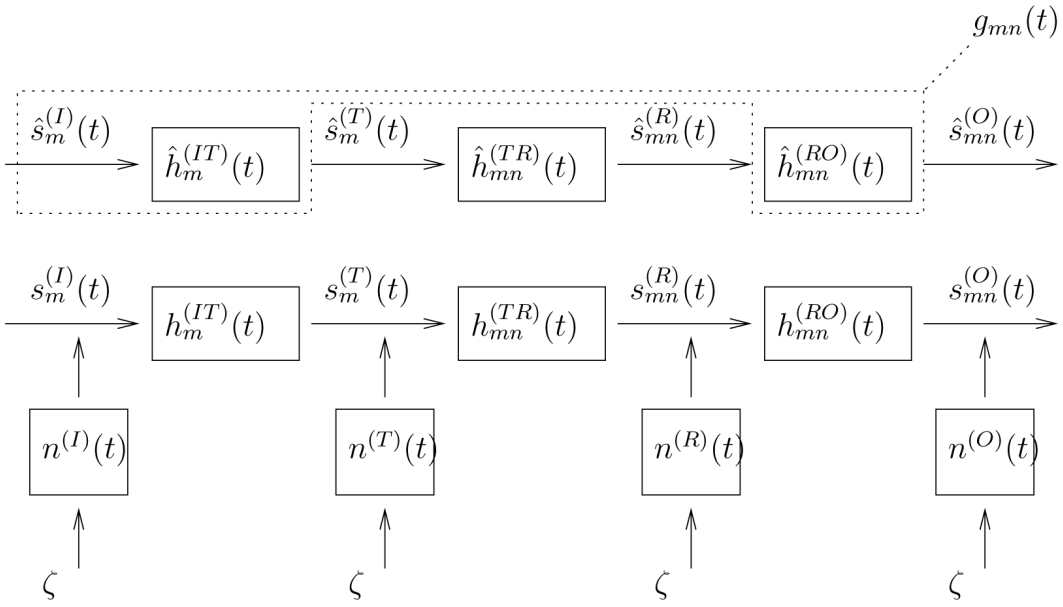

Fig. 3. Chart of theoretical (above) and real (below) model of the NDE system. ζ stands for sources of noise, which are treated as stochastic events.

the transducer models (Rus *et al.*, [10]) since the recorded output signals always follow linear relationships. For this condition, it is always possible to group the signals into a single transfer function of Fourier type using a proper amplitude rescaling and phase shifts. Consequently, it is not necessary to predict the complete transducer transfer function theoretically, but it can be estimated experimentally at the calibration stage.

III. Forward Procedure

A. Measurement Data

In order to eliminate the uncertainties caused by the impact excitation forces or other coherent noises, a convolution-based procedure is designed by comparing the responses of a structure in its undamaged and damaged states. Recall that (1) represents the linear relationships between the output signal $s_{mn}^{(O)}(t)$ recorded by the n-th receiver and the corresponding input signal $s_m^{(I)}(t)$ generated by the m-th transmitter. Based on Fig. 3, these equations can be rewritten as

$$\begin{aligned} s_{mn}^{(O)}(t) &= s_m^{(I)}(t) * h_m^{(IT)}(t) * h_{mn}^{(TR)}(t) * h_{mn}^{(RO)}(t) \\ &= g_{mn}(t) * h_{mn}^{(TR)}(t), \end{aligned} \tag{10}$$

where

$$g_{mn}(t) = s_m^{(I)}(t) * h_m^{(IT)}(t) * h_{mn}^{(RO)}(t). \tag{11}$$

This allows us to describe the response of the complete testing system with a single equation. Taking the inverse of (11), we obtain the response of the specimen as

$$h_{mn}^{(TR)}(t) = g_{mn}^{-1}(t) * s_{mn}^{(O)}(t), \tag{12}$$

which is a property independent of the input signal or intrinsic coherent noises coming from the system. The transfer function $g_{mn}(t)$ can now be used as the input excitation function in our numerical model to obtain the output signal $s_{mn}^{(O)}(t)$ by convolving it with the specimen response $h_{mn}^{(TR)}(t)$. Recall that this is true as long as the model is linear, i.e., it admits the principle of superposition.

B. Real and Theoretical Models

It becomes necessary to study the difference between the real and ideal models in order to assert some hypothesis of the model. For the signals shown in Fig. 3, the real model is described by (10), whereas the ideal model can be represented by the relationship

$$\hat{s}_{mn}^{(O)}(t) = \hat{s}_m^{(I)}(t) * \hat{h}_m^{(IT)}(t) * \hat{h}_{mn}^{(TR)}(t) * \hat{h}_{mn}^{(RO)}(t), \tag{13}$$

where the hats are used to denote the theoretical values.

In our study, we assume that all of the above signal functions or transfer functions are linear, as proved in the previous section. All of them can therefore be treated in the same way as a generic function $f(t)$. This real function is assumed to be linearly proportional to the sum of the ideal function $\hat{f}(t)$ and the bandpass-filtered noise

$$f(t) = z(\hat{f}(t) + n(t) * \lambda(t)), \tag{14}$$

where $n(t)$ is the noise function, and z is the "scaling parameter" or "gain." The output and input signals depend on the variation of the applied pressure, which can be compensated by an arbitrary constant z. The bandpass-filter $\lambda(t)$ is assumed to have a Gaussian probability distribution with average of zero and variance of unity. In other words, this represents a random white noise of unit magnitude.

Note that this function allows us to neglect the phase and sign information in our formulation. Thus, the aforementioned signals and transfer functions can be written in the form

$$\begin{aligned} s_m^{(I)}(t) &= z^{(I)}(\hat{s}_m^{(I)}(t) + n^{(I)}(t) * \lambda(t)), \\ h_{mn}^{(IT)}(t) &= z^{(IT)}(\hat{h}_{mn}^{(IT)}(t) + n^{(IT)}(t) * \lambda(t)), \\ h_{mn}^{(TR)}(t) &= z^{(TR)}(\hat{h}_{mn}^{(TR)}(t) + n^{(TR)}(t) * \lambda(t)), \\ h_{mn}^{(RO)}(t) &= z^{(RO)}(\hat{h}_{mn}^{(RO)}(t) + n^{(RO)}(t) * \lambda(t)), \\ s_{mn}^{(O)}(t) &= z^{(O)}(\hat{s}_{mn}^{(O)}(t) + n^{(O)}(t) * \lambda(t)). \end{aligned} \tag{15}$$

Substituting (15) into (10) and neglecting the higher-order terms of the noise,

$$\begin{aligned} & z^{(O)}\hat{s}_{mn}^{(O)} + z^{(O)}n^{(O)}\lambda \\ &= z^{(RO)}\hat{h}_{mn}^{(RO)}z^{(TR)}\hat{h}_{mn}^{(TR)}z^{(IT)}\hat{h}_{mn}^{(IT)}z^{(I)}\hat{s}_m^{(I)} \\ &\quad + z^{(RO)}n^{(RO)}z^{(TR)}\hat{h}_{mn}^{(TR)}z^{(IT)}\hat{h}_{mn}^{(IT)}z^{(I)}\hat{s}_m^{(I)}\lambda \\ &\quad + z^{(RO)}\hat{h}_{mn}^{(RO)}z^{(TR)}n^{(TR)}z^{(IT)}\hat{h}_{mn}^{(IT)}z^{(I)}\hat{s}_m^{(I)}\lambda \\ &\quad + z^{(RO)}\hat{h}_{mn}^{(RO)}z^{(TR)}\hat{h}^{(TR)}z^{(IT)}n_{mn}^{(IT)}z^{(I)}\hat{s}_m^{(I)}\lambda \\ &\quad + z^{(RO)}\hat{h}_{mn}^{(RO)}z^{(TR)}\hat{h}_{mn}^{(TR)}z^{(IT)}\hat{h}_{mn}^{(IT)}z^{(I)}n^{(I)}\lambda \\ &\quad + H.O.T. \end{aligned} \tag{16}$$

The equality condition in this equation should be independently carried out for the group of terms for any magnitude of noise. Equating the terms without noise and using (13), we obtain

$$z^{(TR)} = \frac{z^{(O)}}{z^{(RO)}z^{(IT)}z^{(I)}}. \tag{17}$$

This unifies the pressure-dependent scaling factor. Equating the terms with the first-order noise, the following relationship is obtained, which provides an additive bound to the effect of noise on the final inverse problem solution:

$$\frac{n^{(TR)}}{\hat{h}_{mn}^{(TR)}} = \frac{n^{(O)}}{\hat{h}^{(O)}} + \frac{n^{(RO)}}{\hat{h}_{mn}^{(RO)}} + \frac{n^{(IT)}}{\hat{h}_n^{(IT)}} + \frac{n^{(I)}}{\hat{s}_m^{(I)}}. \tag{18}$$

C. Undamaged Specimen for Compensation

We define two categories of calibrations, one in the amplitude domain and the other one in the time domain. Both calibrations are referenced to the undamaged calibration specimen.

1. Amplitude Compensation: The function $\overset{\circ}{S}{}_{mn}^{(O)}$ is a measured reference value obtained from an undamaged specimen, and $\overset{\circ}{\tilde{H}}{}_{mn}^{(TR)}$ is the numerically predicted value. These values for undamaged specimens are denoted by the symbol $\circ$. Our goal is to calibrate G for coherent noise, amplitude variations, system function, and the input signal. The function G is defined in (19) as the average of G_{mn} (see (12)) for every impactor and receiver (N^m and N^n, respectively) computed for the undamaged specimen:

$$G = \frac{1}{N^m N^n}\sum_{m,n}\left(\overset{\circ}{\tilde{H}}{}_{mn}^{(TR)}\right)^{-1}\overset{\circ}{S}{}_{mn}^{(O)}. \tag{19}$$

The motivation of averaging is to reduce the coherent noise resulting from the excitation signal by a factor $\sqrt{N^m N^n}$ by assuming Gaussian distribution of the noise.

2. Compensation for Wavespeed: We can also calibrate the wave velocity within the specimen. This compensation is to minimize the internal errors due to any internal inconsistency in the experimental and numerical wavespeeds. Furthermore, it is advantageous that we do not need to have accurate wavespeed values since they can be self-adjusted. The equation of motion [14], [15] is rewritten as

$$\left(\frac{k_s}{k_p}\right)^2 \nabla(\nabla\cdot u) + \nabla\times(\nabla\times u) + k_s^2 u_{,tt} = 0, \tag{20}$$

where $k_s = (\omega/c_s) = \omega\sqrt{\rho/\mu}$ and $k_p = (\omega/c_p) = \omega\sqrt{(\rho/\lambda + 2\mu)}$ are the wavenumbers, ω is the angular frequency, ρ is the density, and μ and λ are the Lamé constants.

By assuming that the Poisson's ratio is known, the wavespeed ratio remains constant, and we can calibrate a single one c_s as follows:

$$\begin{aligned} c_s' = \alpha c_s \Rightarrow k_s' &= \frac{1}{\alpha}k_s \\ \Rightarrow \left(\frac{k_s'}{k_p'}\right)^2 \nabla(\nabla\cdot u) + \nabla\times(\nabla\times u) + k_s'^2 u_{,t't'} &= 0 \\ \Rightarrow \frac{d}{dt'} = \alpha\frac{d}{dt} \Rightarrow t' &= \frac{1}{\alpha}t. \end{aligned} \tag{21}$$

This means that the wave velocity can be adapted by scaling the time by the factor $(1/\alpha)$. Moreover, the use of signal processing techniques allows us to eliminate the need for new computations. Implementation of this compensation scheme simply consists of finding the minimum of a cost functional, defined as the integral over the time window (TW, specified in next section) of the residual between the synthesized and measured output signals $s_{mn}^{(O)}(t)$ for the known case without defect, as defined above:

$$\min_{\alpha} J = \int_{TW}\left(s_{mn}^{(O)}(t) - \tilde{s}_{mn}^{(O)}(t)\right)^2 dt. \tag{22}$$

D. Boundary Element Method

The boundary element method (BEM) is used because of its advantages over the finite element or other discrete methods. First, the BEM does not require re-meshing of the body domain at each iteration. This not only reduces the computational time but also eliminates small but important perturbations due to the changes of meshes. Second, by reducing the dimension of the problem by one, fine meshes required to represent high frequency waveforms become affordable by using the BEM.

We use the singular formulation of the boundary integral equation (see Dominguez [16]),

$$c_k^i(\mathbf{x})u_k(\mathbf{x}) + \int_\Gamma \left[p_k^i(\mathbf{y};\mathbf{x})u_k(\mathbf{y}) - u_k^i(\mathbf{y};\mathbf{x})p_k(\mathbf{y})\right] d\Gamma(\mathbf{y}) = 0. \tag{23}$$

This equation relates the displacements u_k and the tractions p_k exclusively at the boundaries. The index k stands for the dimensions of the Cartesian coordinates of space. If a complex presentation of fundamental harmonic solutions for p_k^i and u_k^i is used, the solution of this equation yields fundamental harmonic solutions for a single frequency ω. In the boundary integral equation, c_k^i is a geometry-dependent constant, and the integral has the sense of a Cauchy principal value. In implementation, we use the classical conforming discretization scheme with quadratic elements, 8-point Gauss integration after regularization and displaced collocation strategy. The implementation details were developed by Rus [17]. This equation is used for both boundary and internal points [16], [18]. The voids are modeled as stress-free boundaries.

The signals are recorded over a time window of 50 μs using a broadband transducer of 500 kHz. In order to match this sampling condition, the frequency-domain signals are constructed in the sampling range between zero and 4 MHz at the increment of 20 kHz. When the response function is constructed in terms of displacements and tractions, they are Fourier-transformed to obtain the time domain response.

IV. Implementation

A. Procedure

The theory described so far is implemented for evaluating the defect in a specimen using the recorded output signal. Below is the procedure for implementation.

1. **Preprocessing** of experimental signal.
   a) Consider only the time window between 2.5 and 47.5 μs, cropped from the original 50-μs recording period. This avoids mismatch of the ends due to the periodic nature of the Fourier transform.
   b) Join the beginning and end points of the experimental signal by using a linear transition during the last 2.5 μs. This is to avoid perturbing discontinuities.
   c) Displace the signal to zero mean. This eliminates the static components.
2. **Calibration** to synthesize a signal.
   a) Compute $\tilde{H}_{mnj}^{(TR)}$ using BEM for the reference specimen. Each term j is obtained from the solution of a single stationary frequency. The numerical technique, taking into account the boundary conditions and the relationship between the signal and the response ($s_m^{(T)}(t) = q_i(\Gamma_m, t)n_i$ and $s_{mn}^{(R)}(t) = \int_{\Gamma_n} u_i(\Gamma, t)d\Gamma n_i$), has been explained previously.
   b) Resample computed signal $\tilde{h}_{mn}^{(TR)}(t)$ using a set of factors $\alpha_i = (p_i/q)$. A polyphase implementation has been used in this case, with a resampling up between $p_i = \times 90$ and $\times 110$, a resampling down of $q = \times 100$, and an oversampling of $N = \times 10$. An anti-aliasing (lowpass) FIR filter is used to compensate for signal delay after the filter and a Kaiser window with $\beta = 5$ [$w_n = I_0(\beta\sqrt{1 - n^2/m^2})/I_0(\beta)$, where I_0 is the zeroth order Bessel function of the first kind].
   c) Compute $g(t)$, the average of $g_{mn}(t) = {s_{mn}^{(O)}}^{-1}(t) * \tilde{h}_{mn}^{(TR)}(t)$.
   d) Generate the synthesized signal $\tilde{s}_{mn}^{(O)} = g(t) * \tilde{h}_{mn}^{(TR)}(t)$.
   e) Compute the residual $R = s_{mn}^{(O)}(t) - \tilde{s}_{mn}^{(O)}(t)$.
   f) Join the first and last points of the residual R using a linear transition during the last 2.5 μs.
   g) Compute the cost functional $J = (1/2N)\sum_{i=1}^{N} (R)^2$ and find the value that minimizes α_i.

B. Experimental Setup

The previous formulation is used for analyzing the subsurface defect in an aluminum specimen, whose mechanical properties are identified before calibration as $c_p = 6320$ m/s, $c_s = 3130$ m/s, $\rho = 2700$ kg/m^3, and zero damping. We limit ourselves to a 2D problem. For that purpose, a sufficiently wide specimen is used, together with a strip-like defect and line transducers. The accuracy of the simplification of the piezoelectric plate from 3D to 2D can be determined from Johansson *et al.* [19]. The transducers are fabricated by inserting a trapezoidal aluminum wedge between the piezoelectric plate and the specimen, which produces contact on the line. The design of this wedge is well described by Rus *et al.* [10].

Fig. 4 shows the geometry of the specimen used in the experiments. The dimensions of the specimen are sufficiently large so that any signal reflected from the boundaries appears outside of the range of interest. A pair of 500-kHz central frequency wideband transducers from Panametrics are used in transmission mode. Table I tabulates the setup configuration of the measurement system used in the experiments shown in Fig. 5.

Computational methods always add a source of errors, which should be reduced by mesh refinement to a negligible magnitude, as compared to other experimental errors, at the cost of an increased computing time. Fig. 6 shows a sensitive detail of the superposed signals computed by two different boundary element meshes, which serve as a bound of the numerical error. The finer mesh of 60 elements is adopted, providing a maximum size of 2 mm in order to obtain an accuracy of the order of 1% by a refinement test. The figure also shows a picture of the ultrasonic pulse at a particular instant, and how it interacts with the defect.

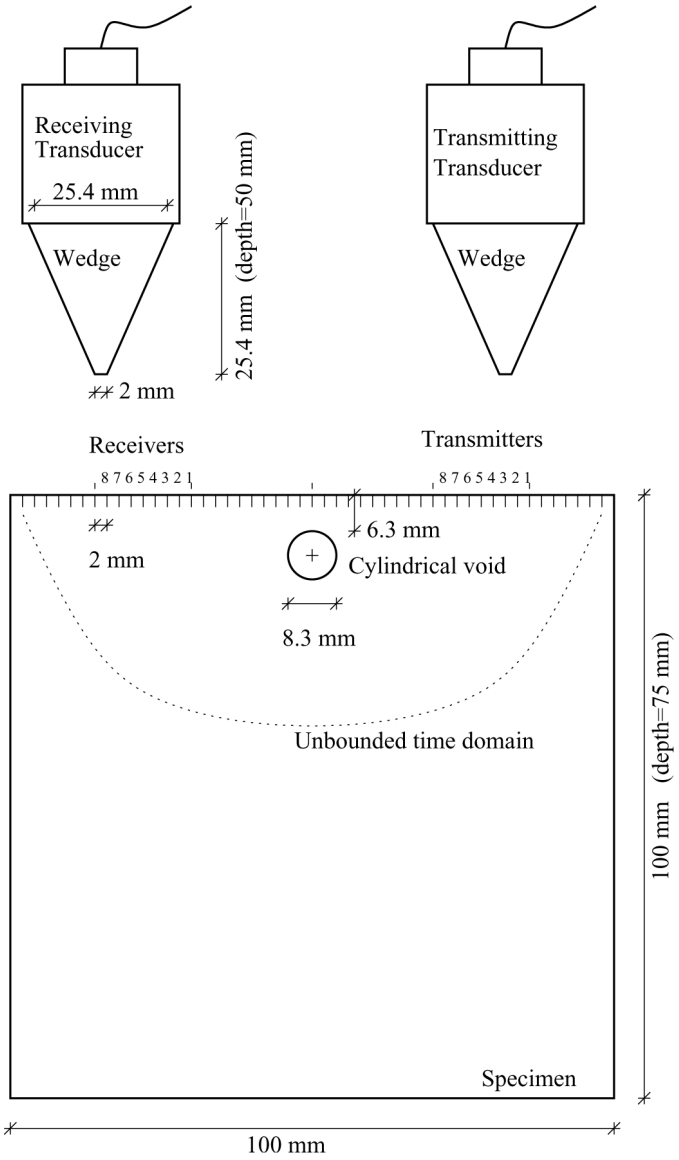

Fig. 4. Geometry of the model.

V. Experimental Results

Fig. 7 shows the response $h_n^{(TR)}(t)$ obtained by the BEM for the undamaged and the defective specimen. Fig. 8 shows the comparison between the experimental signal and the signal synthesized by the previous computation for the undamaged specimen as well as for the damaged one. The difference due to direct subtraction appears to be small in the first case, but considerable for the defective specimen. Notice that the signals for the reference and defective specimens are similar looking because the main part of the signal consists of surface wave, which carries no information about the defect, whereas the P- and S-wave reflections from the defect are small and not distinguishable by the raw eye. It will be shown in the next part that the proposed inversion technique is robust enough to overcome this drawback.

The technique is valid not only for side-drilled holes, but also for straight or curved cracks with any orientation,

TABLE I
Configuration of the Experimental Setup.

Wave generator	
Waveform generator model	HP 33120A
Repetition rate	50 Hz
Burst cycle	1
Pulse height	500 mV
Frequency	500 kHz
Burst shape	Spike pulse
RF power amplifier model	ENI 2100L
Amplification	+50 dB
Frequency range	10 kHz − 12 MHz
Oscilloscope	
Oscilloscope model	Agilent 54624A
Amplitude division	100 mv/div
Time division	5 μs/div
Sampling rate	25 ns
Time trigger delay	−29 μs
Trigger level	25 mV
Averaging	64×

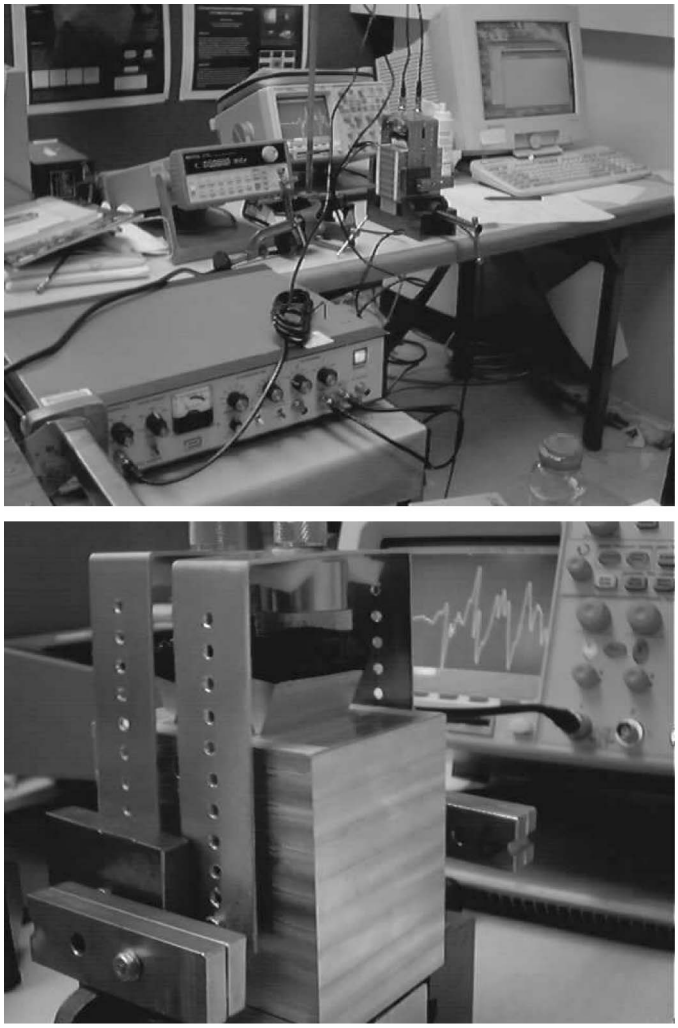

Fig. 5. Experimental setup.

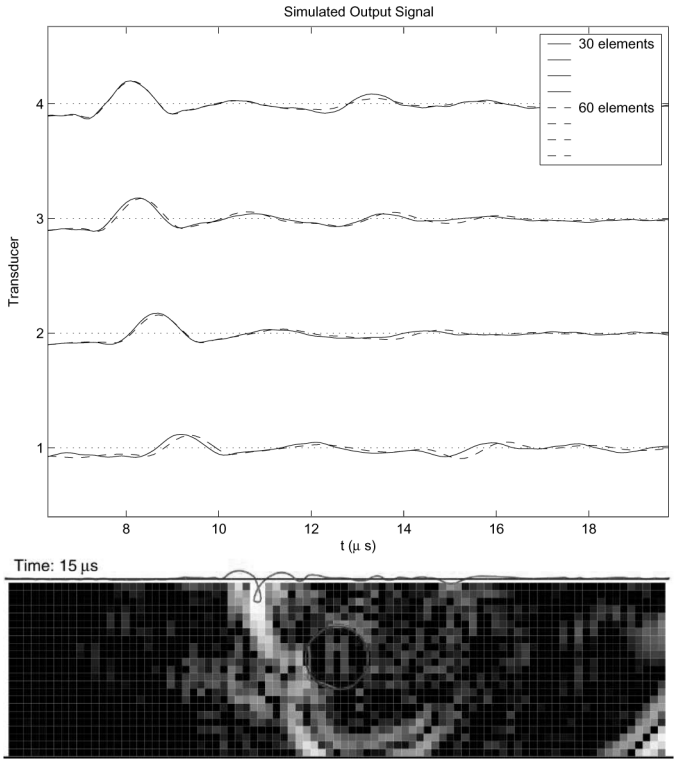

Fig. 6. An example of computation with increasingly refined boundary element discretization (zoomed over a sensitive area). Note the details of the interaction of the P and S waves with the defect and the surface waves.

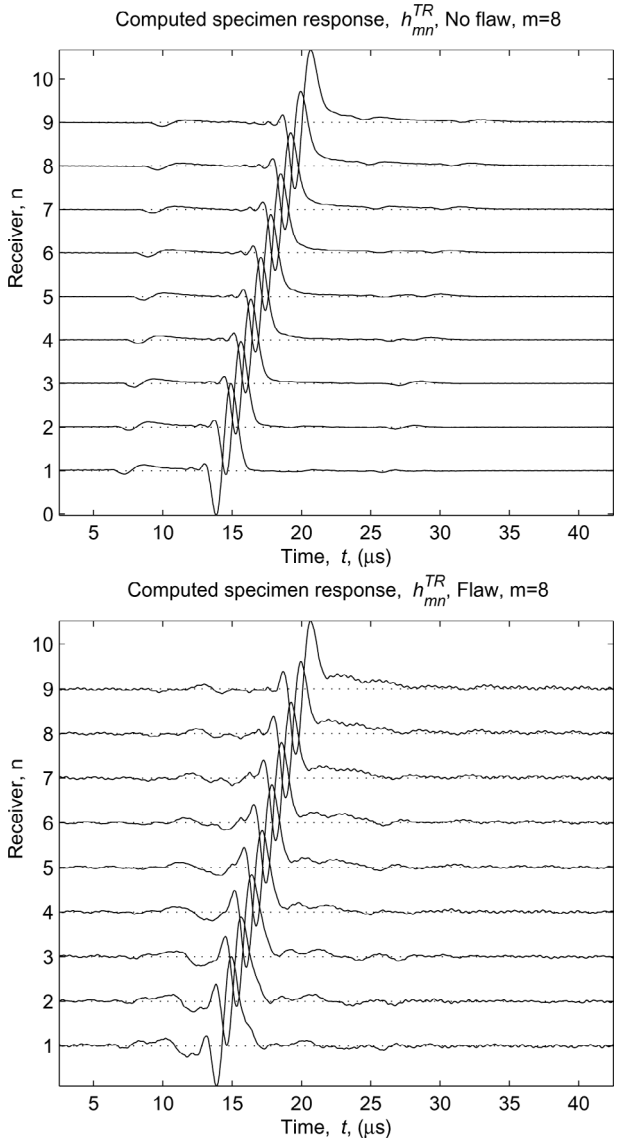

Fig. 7. Computed response of the specimen system, prior to convolution. Response at all 9 receivers from one of the 9 transmitters (note that only 8 receivers and transmitters were used to simulate the array, and the 9th one was recorded only for safety and preventive reasons, but never used in any calculation). Top: case with no defect. Bottom: case with defect.

or for inclusions (which are more complicated to validate experimentally), using the current boundary element code, and can be extended to other formulations of continuum or discrete damages. Finally, Fig. 9 shows the optimization for α and the wavespeed self-compensation used in the previously synthesized signals.

VI. Conclusions

A model-based defect-detection method for analyzing the signals using an array of ultrasonic sensors is developed. In the first part, the model is implemented and two calibration techniques are introduced to predict the model for the actual specimen. These techniques are actually used in the second part for solving the inverse problem and finding the parameters that describe the defect.

This work is understood as an initial study aimed at testing a new concept in NDE, a model-based inverse problem solution. Being still far from practical application, the coming steps in its development are extending the types and parametrization of damage, the efficient boundary element computations, and further study of the noise effects on the probability of detection.

The strengths of the proposed method are as follows: (a) The calibration technique can be processed in both the time and the amplitude domains without all of the parameters being known, due to the abundance of measurements available for the computation. The parameters that do not need to be known include the exact wavespeed, the actual pressure applied to the transducers, their response transfer function, and the input signal. (b) The method is applicable to ultrasound range but is basically applicable to any mechanical wave motion. (c) The BEM is used as a convenient tool for solving the forward problem to model wave propagation in the specimen. Besides the computational speed, the most important characteristic is avoiding the domain mesh, which eliminates numerical perturbations that affect the search procedures. The BEM is accurate and suited for modeling infinite geometries and complicated geometries, as compared to other methods.

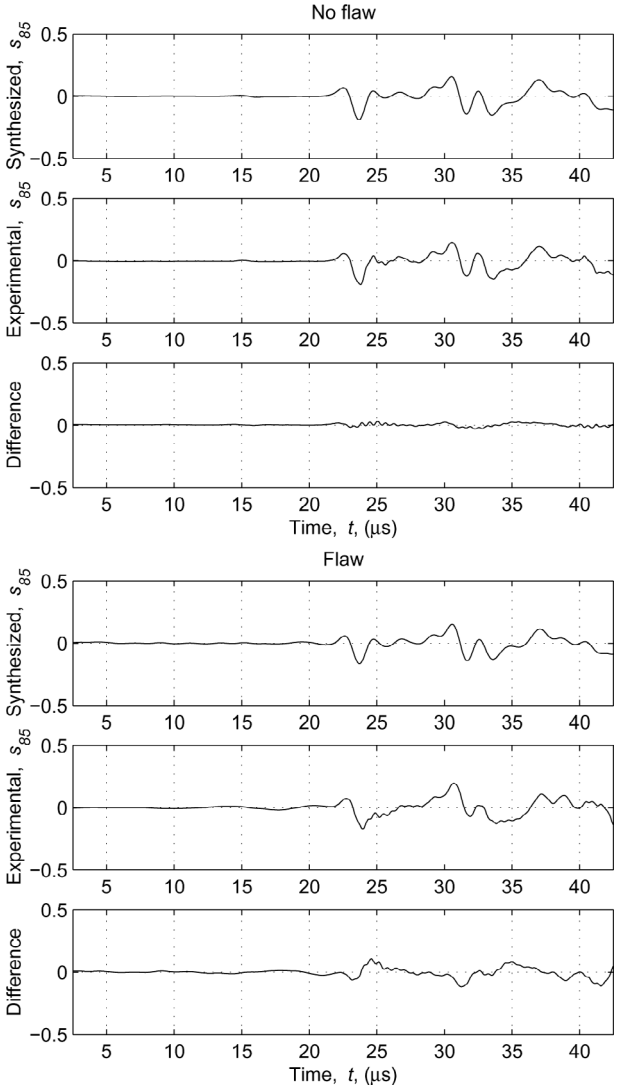

Fig. 8. Comparison of experimental and synthesized signal. Case of a single transmitter and receiver. Top: case with no defect. Bottom: case with defect.

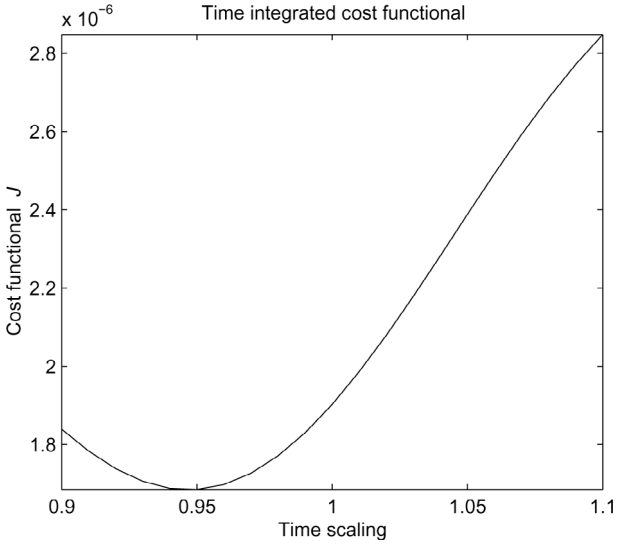

Fig. 9. Wave speed calibration. Minimization of the cost functional for wave celerity compensation.

References

[1] R. K. Miller, *Nondestructive Testing Handbook*. 5th ed. vol. 5, Columbus, OH: American Society for Nondestructive Testing, 1986.

[2] P. N. Marty, M. J. S. Lowe, and P. Cawley, "Finite element predictions of guided ultrasonic wave fields generated by piezoelectric transducers," in *Review of Progress in Quantitative Nondestructive Evaluation*. vol. 20, D. O. Thompson and D. E. Chimenti, Eds. Melville, NY: Amer. Inst. Phys., 2000.

[3] R. Wendel and J. Dual, "Application of neural networks to quantitative nondestructive evaluation," *NDT&E International*, vol. 30, no. 5, p. 323, 1997.

[4] P. Calmon, A. Lhémery, I. Locoeur-Thaïbi, R. Raillon, and L. Paradis, "Models for the computation of ultrasonic fields and their interaction with defects in realistic ndt configurations," *Nucl. Eng. Design*, vol. 180, pp. 271–283, 1998.

[5] A. S. Eriksson, A. Bostrom, and H. Wirdelius, "Experimental validation of utdefect," SKI (Statens Kärnkraftverksinspektion), Tech. Rep. SKI Report 97:1, 1997.

[6] K. Kimoto and S. Hirose, "A numerical modelling of contact shwave transducers," in *Review of Progress in Quantitative Nondestructive Evaluation*. vol. 20, D. O. Thompson and D. E. Chimenti, Eds. Melville, NY: Amer. Inst. Phys., 2000.

[7] L. W. Schmerr, *Fundamentals of Ultrasonic Nondestructive Evaluation*. New York: Plenum, 1998.

[8] J. Zhao, P. A. Gaydecki, and F. M. Burdekin, "A numerical model of ultrasonic scattering by a defect in an immersion test," *Ultrasonics*, vol. 33, no. 4, pp. 271–276, 1995.

[9] C. R. Hill, J. C. Bamber, and G. R. Haar, Eds. *Physical Principles of Medical Ultrasonics*. 2nd ed. New York: Wiley, 2004.

[10] G. Rus, S. Wooh, and R. Gallego, "Analysis and design of wedge transducers using the boundary element method," *J. Acoust. Soc. Amer.*, vol. 115, pp. 2919–2927, 2004.

[11] W. Sachse, "Transducer considerations for point-source/point-receiver materials measurements," *Ultrasonics*, vol. 25, no. 6, p. 356, Nov. 1987.

[12] Y. C. Lee and S. H. Kuo, "A new point source/point receiver acoustic transducer for surface wave measurement," *Sens. Actuators A*, vol. 94, pp. 129–135, 2001.

[13] S. Ying, "Single narrow beam ultrasonic transducer with conical and wedge shaped collimators," *Ultrasonics*, vol. 5, no. 4, p. 276, Oct. 1967.

[14] I. A. Viktorov, *Raleigh and Lamb Waves*. New York: Plenum Press, 1967.

[15] K. F. Graff, *Wave Motion in Elastic Solids*. Mineola, NY: Dover Publications, 1975.

[16] J. Domínguez, *Boundary Elements in Dynamics*. New York: Elsevier, CMP, 1993.

[17] G. Rus, "Numerical methods for nondestructive identification of defects," Ph.D. dissertation, Universidad de Granada, E.T.S.I. Caminos, C. y P., June 2001.

[18] G. Rus and R. Gallego, "Optimization algorithms for identification inverse problems with the boundary element method," *Eng. Anal. Boundary Elements*, vol. 26, pp. 315–327, 2002.

[19] G. Johansson and A. J. Niklasson, "Approximate dynamic boundary conditions for a thin piezoelectric layer," *Int. J. Solids Struct.*, vol. 40, no. 13–14, pp. 3477–3492, 2003.

Guillermo Rus received his Ph.D. degree in numerical methods for nondestructive identification of defects in 2001 at the University of Granada, Granada, Spain. He worked at the NDE Laboratory at the Massachusetts Institute of Technology, Cambridge, MA, as a Fulbright Postdoctoral Fellow during 2002–2003. He was also a visitor at the University College London (UK), Chalmers Technical University, Linkoping Institute of Technology (Sweden), Ecole Polytechnique (France), and the University of Alicante and the University Miguel Hernández (Spain), supported by different grants. He teaches structural mechanics as an associate professor at the University of Granada, where he is also promoting the Nondestructive

Evaluation Laboratory. Dr. Rus is the recipient of several prestigious awards, including the Juan Carlos Simó for young researchers in numerical methods (SEMNI), and is a Fellow of the Wessex Institute of Great Britain.

Shi-Chang Wooh is President of Remos Technologies, Inc. He obtained his Ph.D. degree in theoretical and applied mechanics from Northwestern University, Evanston, Illinois. Before founding Remos Technologies, he was an Esther and Harold E. Edgerton Associate Professor at the Massachusetts Institute of Technology. His research areas encompass a broad spectrum of mechanics, including wave propagation and ultrasonics, nondestructive evaluation, sensor technology, composite materials and structures as well as embedded systems design and applications. Dr. Wooh is the recipient of several prestigious awards, including the Esther and Harold E. Edgerton Development Chair and NSF CAREER award. He has coauthored more than 140 technical papers.

Rafael Gallego is Professor and Head of the Department of Structural Mechanics of the University of Granada. He graduated and obtained his Ph.D. degree at the University of Sevilla, Sevilla, Spain, and was a Fulbright Postdoctoral Fellow at Brown University, Providence, RI. His active research field focuses on the application of the boundary element method in damage evaluation and characterization of advanced materials, particularly using topological and geometrical sensitivity. He is co-author of seven books and more than 40 papers in international journals.